RSC Advances

In vivo facile fabricated hypertrophic scars model through continuous gradient elastic tension driven

Journal:	*RSC Advances*
Manuscript ID	RA-ART-09-2015-018287.R1
Article Type:	Paper
Date Submitted by the Author:	03-Nov-2015
Complete List of Authors:	Cheng, Liying; Shanghai Ninth People's Hospital Shanghai Jiao Tong University, School of Medicine, Department of Plastic and Reconstructive Surgery Sun, Xiaoming; Shanghai Ninth People's Hospital Shanghai Jiao Tong University, School of Medicine, Department of Plastic and Reconstructive Surgery Yu, Jia; The First Affiliated Hospital of Soochow University, Department of Orthopedics Guo, Qianping; The First Affiliated Hospital of Soochow University, Department of Orthopedics Jin, Rong; Shanghai Ninth People's Hospital, Shanghai Jiao Tong University, Department of Plastic and Reconstructive Surgery Sun, Baoshan; Shanghai Ninth People's Hospital, Shanghai Jiao Tong University, Department of Plastic and Reconstructive Surgery Shi, Yaoming; Shanghai Ninth People's Hospital, Shanghai Jiao Tong University, Department of Plastic and Reconstructive Surgery Cui, Wenguo; The First Affiliated Hospital of Soochow University, Department of Orthopedics Zhang, Yuguang; Department of Plastic and Reconstructive Surgery, Shanghai Ninth People's Hospital, Shanghai Jiao Tong University, School of medicine
Subject area & keyword:	Mechanics < Physical

In vivo facile fabricated hypertrophic scars model through continuous gradient elastic tension driven

Liying Cheng[a], Xiaoming Sun[a], Jia Yu[b], Qianping Guo[b], Rong Jin[a], Baoshan Sun[a], Yaoming Shi[a], Wenguo Cui[b*], Yuguang Zhang[a*]

[a] *Department of Plastic and Reconstructive Surgery, Shanghai Ninth People's Hospital, Shanghai Jiao Tong University, School of medicine, 639 Zhi Zao Ju Road, Shanghai 200011, P.R. China.*

[b] *Department of Orthopedics,The First Affiliated Hospital of Soochow University, Orthopedic Institute, Soochow University,708 Renmin Road , Suzhou , Jiangsu 215006 , P. R. China.*

* *Corresponding authors:*

Fax/Tel: +86-21-63089562, +86-512-67781420.

E-mail: zhangyg18@126.com (**YG Zhang**);wgcui80@hotmail.com (**WG Cui**)

This work was supported in part by National Natural Science Foundation of China (81372703 and 51373112), Jiangsu Provincial Special Program of Medical Science (BL2012004), Jiangsu Provincial Clinical Orthopedic Center, the Priority Academic Program Development of Jiangsu Higher Education Institutions (PAPD).

List of abbreviations:

Continuous gradient elastic tension driven group (CG-ETD)

Continuous gradient elastic tension driven (CG-ETD)

Early elastic tension driven group (E-ETD)

Red Duroc pig (FRDP)

Hypertrophic scars (HScs)

Later gradient elastic tension driven group (LG-ETD)

Later gradient elastic tension driven (LG-ETD)

Phosphate-buffered saline (PBS)

Standard deviation (SD)

1 Introduction

Hypertrophic scars (HScs) following the wound healing process are challenging problems facing the plastic surgeon. All adult human wounds heal with some degree of scar formation after the estimated 230 million major surgical procedures performed worldwide each year [1, 2]. HScs usually cause both cosmetic deformities and functional impairment, which can cause considerable morbidity. Current treatment options for HScs remain inadequate due to our limited understanding of scar pathophysiology. Explorations on HScs have been very slow due to the lack of a simple and effective animal model. Current available animal models for HScs study are either too complicated or too costly, and cannot similarly mimic human HScs process. Studies on HScs have relied mostly upon human pathological samples. Such samples preclude investigation of the initiating factors responsible for HScs development, because they only represent the end point of the HScs process. Therefore, fabricating a proper and reliable animal HScs model is definitely one important and essential challenge for HScs study [3, 4].

Presently, the HScs animal models mainly include rabbit [5-9], Female Red Duroc Pig [10-13], guinea-pig [14], rat [15-16], and mouse [17-19]. For example, the rabbit ear model, involves a small, full-thickness wound overlying the cartilage, which serves as a popular HScs model, due to delayed healing of an excisional wound on the ear cartilage surface. However, rabbit ear HScs model was different from the wounds in the skin of human which is not often overlying the cartilage [5-8]. The female, red Duroc pig (FRDP) reported by Kathy Q, Zhu was used to study the similarity of

hypertrophic scarring between human and red Duroc pig resulting from excisional wounds at different depth; however whether the scars in FRDP resemble human HScs remains controversial [11-13]. Although the understanding of the pathology of HScs evolves with the development of animal models [20], still none of these animal models can completely mimic the development of human HScs.

From clinical research, we have found that HScs usually occur in chest, joints, upper back, shoulder, deltoid area in the upper limbs where there is tension [21]; On the contrary, in the less tension area, such as eyelids, genital organs, cornea, and mucosa, the scars were less obvious [22, 23]. Whereas, in the mammal animals any wound can heal without scars. This might be because that, there is a panniculus carnosus in the deep dermis, which is very loose, elastic and of great mobility, and can easily extend to cover the wound, which further cause the absence of tension in the skin wound [5]. Yet, in human there is no such panniculus carosus, thus there is tension of various degrees in the skin wound, which results into HScs. Therefore, tension might be one important factor in HScs formation. Gurtner et al have developed a mechanical load murine hypertrophic scar model, and elucidated some mechanism of mechanotransduction in murine fibroblasts and hypertrophic scar in recently years. However, the mechanical loading device is complicated to apply, very expensive, and may not be economic or suitable for large numbers of animal study. Furthermore, the relationship of mechanical load stimulating mode and hypertrophic scar formation has not been explored so far and remains unknown [24-27]

In this study, a facile and economical gradient elastic tension driven was applied on

the wounds to exclude the tension-free status of rat's wounds, and a new and facile rat scar model was created. To specify the best timing for reducing wound tension to reduce HScs formation, we further investigated whether different tension driven mode applied in different phases of wound healing has any different impact on the HScs formation. Further histological characters were studied to compare the similarity of this rat scar and human HScs, which showed that they are of high similarity.

2 Materials and methods

2.1 Animals and Methods

Five-week-old Sprague–Dawley (SD) rats, female, weighing 180–250 g, were purchased from Shanghai Animal Center, Chinese Academy of Science. The Institutional Review Committee of Shanghai Jiao Tong University, School of Medicine approved all animal study protocols, and the study was strictly carried out with the approval of the Animal Experimentation Ethics Committee of Shanghai Jiao Tong University, School of Medicine. All animal treatments were implemented strictly in accordance with international ethical guidelines and the National Institutes of Health Guide with regard to the use and care of laboratory animals.

2.2 Fabrication of HScs model on rat skin

For the surgical procedure, animals were anesthetized with an intraperitoneal injection of 10% chloral hydrate (40 ml/kg). The dorsal skin was shaved with a shaver. Surgical sites were disinfected using iodine ethanol, and then wiped with 70% ethanol. Two 2 cm linear full-thickness incisions (2 cm apart) were made on the dorsum skin of the rats and then sutured with 3-0 nylon sutures. Four clasps were fixed near each linear

incision, with 2 on each side, 0.5 cm apart from the incision, respectively. An elastic tension driven applier was hooked on each clasp. Then tension could be adjusted by shortening the elastics. An elastic board (10 cm * 6 cm) was fixed by interrupted suturing to the skin on the abdomen to avoid any tension or tighten of the abdomen, thus the animal's moving and food-digesting won't be affected by the elastic tension driven. The rats of all groups awoke 1-2 hours after the operation; all behaved as usual and had normal eating and drinking (Fig. 1).

2.3 Study design

A total of 80 SD rats were randomly divided into four groups (group A, B, C, D), each with different tension driven mode. Tension was measured using a tensionmeter (Fig. 1).

Group A (Control group, n=20): no tension was applied on the incisions, 4 clasps ere fixed on each linear incision as described above. The sutures were removed from the wounds on post-operation day 7 (Day 7).

Group B (Early elastic tension driven group, E-ETD, n=20): Each incision was applied with 2N elastic tension driven after suturing. Both the sutures and the tension were removed from the wounds on post-operation day 7 (Day 7).

Group C (Later gradient elastic tension driven group, LG-ETD, n=20): No tension was applied on the incisions during the first 7 days after incision. The sutures were removed from the wounds on Day 7; meanwhile each incision was applied with 3N elastic tension driven. The tension was added to 4N on Day 14, 5N on Day 21, and removed on Day 28.

Group D (Continuous gradient elastic tension driven group, CG-ETD, n=20): 2N elastic tension driven was applied on the incisions during the first 7 days after incision. The sutures were removed from the wounds on Day 7. The elastic tension driven was added to 3N on Day 7, 4N on Day 14, 5N on Day 21, and removed on Day 28.

A neck collar was fixed on the neck to avoid the circumrotation of the neck and bitten of the sutures or the elastics. Also an elastic board was fixed on the abdomen to avoid any tension or tighten of the abdomen. Animals from each group were sacrificed on day 7(n=5), day 14(n=5), day 28(n=5), and day 56(n=5) for macroscopic, histological, and molecular examination, respectively.

2.4 Finite element analysis of elastic tension driven.

The rat skin was modeled as two-dimensional shell, assuming a homogeneous, isotropic, linearly elastic material with Young's modulus of 0.4 MPa and Poisson's ratio of 0.49.

An 8.0 x 3.0 cm^2 section of skin was modeled with two quadrate (2.0 x 1.0 cm^2) areas representing the elastic tension driven applied rat skin area. The tensile forces were applied according to experiment protocol (from 0N to 5N) and the outside boundaries of the composite were left unconstrained, corresponding with the loose skin of the actual rat dorsum skin. The finite element (FE) package, ABAQUS v6.11 (Simulia, Dassault Systems, USA) was used for the creation of the FE mesh and implicit solver was employed for the stress/strain distribution analysis.

2.5 Histological analysis of scar width and epidermal thickness

Scar samples at various time points were fixed in 4% paraformaldehyde in

phosphate-buffered saline (PBS) for 24 hours at room temperature. For tissue sectioning, the harvested scar tissues were cut at the middle, perpendicular to the incisional line. Sections of 5 μm were subjected to hematoxylin & eosin (H&E) or Masson's trichrome staining, or toludine blue staining. The Trichrome Stain Kit (Modified Masson's) (Atom Scientific, USA) was used for Masson's trichrome staining.

After being stained with H&E, tissue sections at the central wound area were observed under a microscope (Nikon, Japan) at a 20 ×, 100 × and 400 × magnification, and the images were digitally recorded into a computer by the Image-Pro Plus system (Media Cybernetics, Silver Spring, MD). The scar width was determined by measuring the distance between two scar edges located at the middle point between the epidermis and the panniculus carnosus (Fig. 5 B b). To determine the variation of scar width, the scar tissues of each group were sectioned at three different locations that were 100 mm apart (Fig. 5A). The epidermis was measured for thickness at the middle of the scar (Fig. 5B a) [28].

2.6 Analysis of TGF-β1，myofibroblasts and blood vessels.

Immunohistochemistry was performed on 4-μm-thick paraffin-embedded tissue sections. The sections were dewaxed, and endogenous peroxidase activity was quenched with 3% hydrogen peroxide for 10 min, followed by blocking with the corresponding serum from a secondary antibody raised animal species for 1 hour. Slides were then incubated overnight at 4 ℃ with the primary antibody mouse anti-TGF-β1 antibody (1:25, proteintech group, USA) and mouse anti-a-SMA

antibody (1:600, sigma, USA) diluted in the blocking serum，respectively,. After several washes with PBS, the tissue sections were incubated with peroxidase-conjugated goat anti-mouse polyclonal antibody (DAKO, Carpinteria, CA) at a dilution of 1:200 in PBS for 30 min at 37 °C. After several washes in PBS, the signals on the tissue were revealed by incubating with DAB in PBS for 5-10 min, followed by hematoxylin counterstaining. All the tissue sections were observed under a microscope at 100 × and 400 × magnification, and the images were digitally recorded into a computer by the Image-Pro Plus system. A blinded observer counted TGF-β1-positive cells， and a-SMA positive cells in the dermal layer of scars in five random high-power (400 ×) fields from each section, respectively [29]. The corresponding area on the a-SMA stained section was counted by the Chalkley grid method.

2.7 Analysis of mast cells in the scars

Toludine blue staining was used for mast cell detection [2]. Briefly, 5-μm-thick paraffin sections, described previously, were deparaffinized and rehydrated. Sections were stained in toludine blue for 20 min, then washed in distilled water and dehydrated. The sections were cleared in xylene, cover-slipped and then examined at 100 × and 400 × magnification. Mast cells were identified by characteristic morphology of the granules. A blinded observer counted the number of mast cells in the scar tissue in five random high-power (400 ×) fields from each section. Only intact mast cells with distinct blue staining were counted.

2.8 Statistical analysis

Each experiment was carried out in triplicate or quintuplicate. The values were expressed as mean ± standard deviation (SD). Statistical analysis was performed using ANOVA with Tukey-Kramer multiple comparisons in SAS. A value of $p < 0.05$ was considered statistically significant.

3 Results

3.1 Rat skin HScs model through elastic tension driven

A facile fabricated rat skin HScs model was constructed using the method described in subsection 2.2 (Fig. 1 A & B), and different modes of elastic tension driven was applied in the wounds as described in subsection 2.3 (Fig.1 D). Elastic tension was adjusted by shortening of the elastics, and the tension was measured by a tensionmeter (Fig.1 C). The hand-made neck collar fixed well on the neck, and successfully avoided the circumrotation of the neck and bitten of the sutures or the elastics. The elastic board fixed on the abdomen successfully avoided any tension or tighten of the abdomen, thus the rats can eat and drink normally. All the above measures contributed together to make this model a stable Rat HScs model.

3.2 Finite element prediction of the wound skin tissue response in rats.

Figure 2 A shows the tensile stress distributions of the rat wounding skin after applied with different elastic tensile forces. As could be seen, with absence of elastic tensile force, the wound healed naturally without stress. However, as the elastic tensile force increased, the tensile stress and scar area increased remarkably at the wound region. The largest tensile stress is predicted over 0.42 MPa at wounding skin when applying 5N tensile force. This phenomenon indicated that under CG-ETD, obvious tensile

stress concentration could appear at the wound skin.

The von Mises stress distribution was shown in Fig. 2 B. When no elastic tensile force was applied, the rat skin remained in an elastic state, and there was no deformation energy. However, when applied with increased elastic tensile forces, the skin stored larger deformation energy and all concentrated at the wound area (Max. von Mises stress=0.24 MPa). These results predicted that when applying CG-ETD, the high tensile stress and the deformation energy were all concentrated at wound skin.

3.3 Macroscopic observations

All the wounds healed without complications. In all groups, wounds were covered by a blood clot on post-operation day 3. No wound reopening was observed in this study.

In the control group, the wound healed completely at week 1 with a narrow scar, without inflammatory erythema. This scar became narrower in 2 weeks, and gradually became invisible at week 3. The scar couldn't be discerned at week 8.

In the early elastic tension driven group (E-ETD), the wound was infiltrated by inflammatory erythema at week 1, which was then disappeared after the tension was removed. The wound healed with a faint red scar on Day 9, which gradually turned faint after the tension was removed. Finally it became a narrow faint linear scar. This scar could not be easily distinguished from the normal skin.

In the later gradient elastic tension driven group (LG-ETD), the wounds healed at week 1. After applied with tension, there is mild erythema and edema, which then turned into a red and hard scar, with absence of hair and with contracture in the scar edges. After the tension was released from week 5, the red scar gradually turned white,

stiff, and elevated a little bit compare to the surrounding skin. This pathology process was similar to that of human HScs.

In the continuous gradient elastic tension driven group (CG-ETD), the wound was surrounded by inflammatory erythema in at week 1. It healed with a red and hard scar, with absence of hair and contracture in the scar edges on day 9. After the tension was released from week 5, the red scar gradually turned white, stiff, and elevated a little bit, which was similar to the LG-ETD group, but with wider scars, which is more similar to human HScs.

As can be seen, tension applied in rats' wounds can lead to scar formation; however, the scars were different as different tension driven modes were applied in different phases of wound healing. Mechanical tension applied in the early phase of wound healing (E-ETD) can result in linear scar formation; while LG-ETD and CG-ETD groups can lead to HScs formation. The scar in the CG-ETD group is the widest (Fig. 3).

3.4 Histological characteristics

H&E staining of tissue sections at different time points was examined to observe the healing process and the histological characteristics of the scars. Scar width in four groups was also measured and compared.

Histological analysis showed that at Week 1, the wound in the control group and the LG-ETD group healed with complete epithelialization and moderate inflammatory cell infiltration. The wounds in the E-ETD group and CG-ETD group were still filled with a blood clot with numerous inflammatory cells. The epithelium had migrated for

a certain distance along the wound edge among the blood clot and the dermis, but the epithelium of the two edges did not connect with each other. Abundant inflammatory cells could be seen in the dermis of the wounds.

At week 2, the wounds were all healed, with the wound epithelium progressed across the wound bed. All the wounds healed with scar, with the classic histological features of human HScs, such as hypertrophy of fibroblasts, accumulation of collagen, and absence of skin appendages. The scar in the CG-ETD group is the widest, while the scar in the control group is the narrowest.

At week 4, obvious scars could be observed in the E-ETD, LG-ETD and the CG-ETD groups, which were characterized by increase of fibroblasts and accumulations of fine collagen fibrils, dermal nodules in the dermis, indicating excessive cell proliferation and increased new collagen deposition [30]. The scars in the control group is narrow, and were not present with so much hypertrophic fibroblasts infiltration, which is different from that of the tension driven groups (Fig. 3). The scar in the CG-ETD group is the widest, of about 12 folds of that of the control group, which is the narrowest.

At week 8, the HScs became much wider in the LG-ETD group, and the CG-ETD group. On the contrary, the scar in the E-ETD group became narrower than that of week 4. The scars in the control group became even narrower, and could hardly be observed. The scars in the tension driven groups were still characterized by hypertrophy of fibroblasts, accumulations of fine collagen fibrils, dermal nodules in the dermis, and absence of skin appendages [30]; while in the narrow scar of the

control group, there was neither hypertrophy of fibroblasts nor accumulation of collagen, with hair follicles and sebaceous glands gradually grown in. The scar in the CG-ETD group is the widest, of about 26 folds of that of the control group, which is still the narrowest (Fig. 4).

3.5 Quantitative analysis of scar width

The scar width was quantified by measuring the distance between two scar edges located at the middle point between the epidermis and the panniculus carnosus as described previously (Fig. 5 A & B) [28].

The quantification results were shown in Fig. 5. As could be seen, in week 1, the scar width in each group had no significant differences ($p > 0.05$). In week 2, the scar width in the tension driven groups (E-ETD, LG-ETD, CG-ETD) were much wider than the control group. In week 4, the scar widths of the E-ETD group (group B), the LG-ETD group (group C), and the CG-ETD group (group D) were 4, 9, and 12 folds of that of the control group, respectively. The scar widths of the LG-ETD group, and the CG-ETD group became wider as time went by, while the scar widths of the control group, and the E-ETD group became narrower. Till week 8, the scar widths of the E-ETD group, the LG-ETD group, and the CG-ETD group were 3, 10, and 26 folds of that of the control group respectively (Fig. 5.).

3.6 Epidermal thickness

The integrity and thickness of epidermis is a feature of HScs. Therefore the epidermis was measured for its thickness at the middle of the wound or scar, as was described in subsection 2.5 (Fig. 5B, a). Figure 6 shows the growth status of the epidermis in each

group at different time points (Fig. 6, B), and the structure of the epidermis in each group at week 4 (Fig. 6, A). As could be seen, the early wounds had thicker epidermis than that of the later wounds/scars in the four groups. Noticeably, the epidermis was much thicker in the tension driven groups (E-ETD, LG-ETD, CG-ETD) than the control group at each time point. The epidermis is the thickest in the CG-ETD group, and thinnest in the control group. This change lasted till week 8 with significant differences ($p < 0.05$). These results indicated that tension could induce thickening of the epidermis of scar, which is one obvious feature of HScs.

3.7 Mature collagen deposition and structure.

Dense, compact collagen deposition and disorganized collagen structure is another feature of HScs. To assess the accumulation and the organization of the dermal collagen in four groups, sections were subjected to Masson's Trichrome stain (Fig. 7). All the four groups showed accumulation of fine collagen fibrils in the dermis in week 4, reflecting the increased new collagen deposition. The collagen deposition area in the control group was much smaller and the collagen structure is much more organized than the tension driven groups. The collagens in the LG-ETD and CG-ETD group were dense and compact, with much more abundant fibroblasts, and with a distinct margin between the normal dermis at the wounds, which were quite similar to human HScs. The structure and the character of the HScs in the tension driven groups lasted, while in the control group, the scar remodeled into a relatively organized and loose structure, approaching a normal dermal structure in week 8. These results demonstrated that this tension related scar formation model can mimic, to a certain

extent, the abnormal matrix remodeling process that generally occurs in human HScs formation.

3.8 Expression of TGF-β1.

The development of HScs is often linked to the over-expression of TGF-β1 [29]. Elevated levels of TGF-β1 are found in the serum of recovering burn patients [31]. Hypertrophic scars stain more intensely for TGF-β1 than normal skin samples or mature scars do [32]. TGF-β1 is therefore a key cytokine in wound healing and HScs. Hence, TGF-β1 immunohistochemical stain was used to analyze the TGF-β1-positive connective tissue cells expression in each section. As is shown in Fig. 8, high expression levels of TGF-β1 were observed in the whole wound/scar area in week 1 and 2. And then in week 4, the expression level of TGF-β1 got lower in the control group, till week 8 very little of TGF-β1 positive cells could be observed. While in the CG-ETD group, the expression level of TGF-β still stayed much higher than the control group. The result of the continuous high expression level of TGF-β in the CG-ETD group revealed its similarity to the human HScs.

3.9 Quantification of mast cells accumulation.

Scar formation is associated with a prolonged presence of an increased number of mast cells [33]. Previously studies have proved that the HScs contain significantly larger number of mast cells than the other tissues studied, and mature scars contain significantly fewer mast cells than hypertrophic scars [33]. Fig. 9 shows that there are toludine blue-positive cells infiltrating the scars by week 4 (Fig. 9 A). Quantification of mast cell staining indicates that, in week 4, mast cells in scars of group A, B, C, D

are 4.6 ± 1.7, 8 ± 2.3, 9.33 ± 1.4, 12 ± 3 PHF (Per high-power microscopic field), respectively. The number of mast cells in the tension driven groups is higher than the control group at each time point, reflecting the fact that there were more mast cells infiltration in the tension related scars. The number of mast cells is highest in the CG-ETD group (group D). This result was consistent with the human HScs character.

3.10 Quantification of fibroblasts accumulation.

An important part of wound healing and HScs formation is wound contraction, and myofibroblasts are believed to play a crucial role in this process [34-36]. Myofibroblasts are characterized by the expression of a-SMA and are thought to be derived from the fibroblast population under profibrotic growth factor stimulation [36-37]. To compare the myofibroblasts formation in the 4 groups and to further determine the character of scars in the 4 groups, immunohistochemical stain for a-SMA was performed. Immunohistochemistry analysis demonstrated that the CG-ETD group had enhanced a-SMA staining compared to normal rat skin incisional scars (the control group) (Fig. 10).

Figure 10 (A, D) shows a significant increased a-SMA expression in fibroblasts from the CG-ETD group compared to normal rat skin incisional scars (the control group) at week 4. Quantification of a-SMA-positive cells were shown in Fig. 10 (B). As is shown, the number of a-SMA-positive cells in week 1 was higher in the control group than in the CG-ETD group. Then from week 2, the number of a-SMA-positive cell in the control group decreased as time went by, while it increased in the CG-ETD group increased, and stayed almost unchanged in the later time points. Consequently, the

number of a-SMA-positive cells in the CG-ETD group remained much higher than the control group in the later time points. Taken together, these data strongly suggested that the fibroblasts in the tension driven scars in a rat model resemble the phenotype of HScs fibroblasts in terms of a-SMA expression.

3.11 Blood vessels formation

New blood vessel formation is an essential process in wound healing [37]. In HScs tissue, blood flow is increased as measured by laser Doppler, which implies the presence of excessive micro vessels compared with normal scars [38]. To explore the situation of blood vessel formation in scars of the 4 groups, a-SMA immunohistochemical stain was applied (Fig. 10). Fig. 10 (C) shows the quantification of blood vessels in each section at different time points. As could be seen from Fig. 10, the CG-ETD group has more blood vessels formation than the control group at week 4. Fig. 10 (C) suggests that in both the control group and the CG-ETD group, the blood vessels peek at week 2, and gradually shut down at later time points. The number of blood vessels in the CG-ETD group is much higher than the control group in week 2, 4, and 8. This result suggested that the continuous gradient tension related scars got augmented neovascularization, which is one important character in human HScs.

4 Discussions

The importance of mechanical forces in fibrosis have been suggested by a wealth of preclinical and clinical data demonstrating exuberant scarring and fibrosis in anatomical areas with the highest levels of mechanical stress. For example, in heart

failure, physical and chemical signals lead to the activation of cardiac fibroblasts, which involves their differentiation into myofibroblasts and the excessive accumulation of ECM proteins. Mechanical signaling in cardiac tissues provides an example of a medically important fibrotic response that is strongly associated with abnormal cardiac diastolic function [39]. In chondrocytes, mechanical stress induces expression of the ECM remodeling enzymes MMP-13 and ADAMTS-5 [40]. In bone, Wnt/β-catenin signaling is a normal physiological response to mechanical loading of skeletalstructures [41]. In skin, actomyosin-mediated cellular tension enhances tissue stiffness and β-catenin activation, which together contribute to epidermal hyperplasia and tumor growth. Waveform-specific mechanical loads may accelerate skin tissue growth by mechanotransduction. [42] Hypertrophic scar is a skin fibrosis disease, in which mechanical tension play a critical role [43].

Recently, the role of mechanical force is increasingly being recognized in scar pathophysiology, and computer modeling studies have predicted that mechanical tension drives pathologic scarring in humans. Gurtner et al have developed a mechanical load murine hypertrophic scar model. However, the mechanical loading device is complicated to apply, very expensive, and may not be economic or suitable for large numbers of animal study. Also, the relationship of mechanical load stimulating mode and hypertrophic scar formation remains unknown. In this study, we aimed to fabricate a facile mechanical tension load animal model, and to further investigate whether different tension driven modes applied in different phases of wound healing has any different impact on the HScs formation.

The mechanical stress driven device used in this rat model is economical, convenient and easy to manipulate. The results showed that mechanical tension applied at different phase of wound healing could all result in scar formation in this model, which demonstrates that this facile fabricated HScs model has good repeatability. E-ETD could result in linear scar formation, which gradually faded away in the later time points. LG-ETD and CG-ETD could results in HScs formation, which grew wider later. While no tension driven applied group healed normally without scars. The scar formation in the LG-ETD group and the CG-ETD group goes the process of from red to white, and gradually turned raised relative to the surround normal skin, which is very similar to that of human HScs based on clinical and gross morphologic features. The scars were much wider in the CG-ETD group than the LG-ETD group.

HSsc has a unique structural characteristic that is highly vascular with inflammatory cells and fibroblasts contributing to an abundant and disorganized matrix structure [44, 45]. Increased collagen deposition is one of the most predominate features for human HScs [46]. Here in this rat model, we observed abundant collagen deposition. In the E-ETD group, the deposited collagen shows a parallel model, while in the LG-ETD group and the CG-ETD group, the deposited collagen was disorganized, irregularly, and with nodules, which was similar to human HScs. These phenomenons indicated that tension applied in the later phase or continuous tension driven in the whole phase may be the main contributors to the HScs formation.

In HScs, the keratinocytes show increased proliferation and differentiation compared with normal scar keratinocytes [47]. This activated epidermis has reduced IL-1a and

increased PDGF expression compared with normal scar tissue, which probably directly affects collagen production by fibroblasts [48]. Here, from Fig. 6, we could observe that tension driven applied groups got thicker epidermis than the control group at week 4, and at all the other time points.

The TGF-β1 family of growth factors plays a pivotal role in orchestrating normal wound repair and scar formation [49]. The serum of burn patients developing HScs also contains higher levels of TGF-β1 compared with control patients [32]. Non-scarring fetal wounds show a reduced expression of TGF-β1 and a higher expression of fibromodulin, a TGF-β1 binding protein, compared with adult wounds [50, 51]. Accordingly, TGF-β1 is a key cytokine in wound healing and HScs formation. In this study, we found that the tension related scars have significantly increased TGF-β1 expression than the normal skin incision scars at all time points. The TGF-β1 expression in the tension related scars is still high at week 8. This indicates that TGF-β1 may regulate the scar formation in this rat model.

An important character of HScs is contraction, and the myofibroblasts are believed to play a pivotal part in this process. Myofibroblasts are featured by the expression of a-SMA. From Fig. 10, we can observe increased a-SMA-expressing cells in the tension driven related scars than the control group at week 2, 4, 8, indicating that there are more myofibroblasts formation and function during the wound healing and HScs formation. Myofibroblast may contribute to the scar formation in this tension driven related rat scar model.

Besides inflammation, hypertrophy of fibroblasts, thicken of the epidermis, enhanced

vascularization levels is also one important character of HScs. The number of blood vessels was significantly higher in human HScs as compared to normal skin [52]. In this experiment, the tension driven related rat model showed dramatic increases in blood vessel density than the control group, which may contribute to the HScs formation.

These data demonstrate that the reason why mamal animals' wound heals without scars might due to the panniculus carnosus, which causes the tension free state of the mammal animal skin. Thus exclude this tension-free state by applying tension to the wound at different phases of wound healing may result in different scars formation. For example, tension driven applied in the early phase of wound healing can cause narrow linear scar, which gradually fade away as the tension was released. Tension applied in the late phase of wound healing and tension applied in the continuous phase of wound healing can all cause HScs formation. The scar in the CG-ETD group turned out to be wider than the LG-ETD group. And from the above results of this study, we concluded that the mechanisms of this scar formation may be exaggerated inflammation, prolonged re-epithelialization, overabundant extracellular matrix deposition, augmented neovascularization, and atypical extracellular matrix remodeling, which may each play a role individually or sequentially, or synergistically. These mechanisms were currently believed to be the main mechanisms of HScs formation [53].

Through histological detection, we proved that this scar well mimics the human HScs to a certain extent. So this tension driven related rat scar model can be used as a new,

facile, economical and stable animal model for further study of the mechanisms of HScs. However, further researches need to be done to explore more similarities between this scar and human HScs.

The different results of scar formation, due to different kinds of tension in different phase, also give us a hint that decrease the tension in the wound area, especial during the 2-4 weeks after wounding may be a good approach to decrease scar formation.

Conclusion

A new and facile method of gradient tension driven was used in the rat skin wound, and different types of tension driven was applied in different phases of wound healing to explore the relationship between tension and HScs formation. The results demonstrated that tension driven applied in the rat skin wound could induce HScs formation, and the formed scars were quite similar to human HScs. The mechanism of this scar formation is exaggerated inflammation, prolonged reepithelialization, overabundant extracellular matrix deposition, augmented neovascularization, and atypical extracellular matrix remodeling. Continuous gradient elastic tension driven of wound healing can all cause more obvious hypertrophic scars formation than early elastic tension driven and later gradient elastic tension driven. Thus we conclude that this continuous gradient elastic tension driven related rat scar model can be used as a new, facile and economical animal model for hypertrophic scar study.

Acknowledgements

This work was supported in part by National Natural Science Foundation of China

(81372703 and 51373112), Jiangsu Provincial Special Program of Medical Science (BL2012004), Jiangsu Provincial Clinical Orthopedic Center, the Priority Academic Program Development of Jiangsu Higher Education Institutions (PAPD).

Disclosure Statement

The authors declare that they have no conflicts of interest concerning this article.

References

1. Gurtner GC, Werner S, Barrandon Y, et al: Wound repair and regeneration. Nature 1994; 453:314-321.
2. Weiser TG, Regenbogen SE, Thompson KD, et al: An estimation of the global volume of surgery: a modelling strategy based on available data. Lancet 2008; 372:139-144.
3. Sun KK, Lewis WH. Hypertrophic scar: a genetic hypothesis. Burns 1990; 16: 176–178.
4. Tomasek JJ, Petro JA, Eddy RJ. Evidence for the nonmuscle nature of the ‘‘myofibroblast’’ of granulation tissue and hypertropic scar. An immunofluorescence study. Am J Pathol 1998; 130: 252–60.
5. Kloeters , O., Tandara, A., Mustoe, TA. Hypertrophic scar model in the rabbit ear: a reproducible model for studying scar tissue behavior with new observations on silicone gel sheeting for scar reduction. Wound Repair Regen 2007; 15 Suppl 1:S40-45.
6. Lee JP, Jalili RB, Tredget EE, et al: Antifibrogenic effects of liposome-encapsulated IFN-alpha2b cream on skin wounds in a fibrotic rabbit ear model. J Interferon Cytokine Res 2005; 25:627-631.
7. Morris DE, Wu L, Zhao LL, et al: Acute and chronic animal models for excessive dermal scarring: quantitative studies. Plast Reconstr Surg 1997; 100: 674-681.
8. Rahmani-Neishaboor E, Yau FM, Jalili R, et al: Improvement of hypertrophic

scarring by using topical anti-fibrogenic/anti-inflammatory factors in a rabbit ear model. Wound Repair Regen 2010; 18: 401-408.

9. Xu TM, Xin Y, Cui MH, et al: Inhibitory effect of ginsenoside Rg3 combined with cyclophosphamide on growth and angiogenesis of ovarian cancer. Chin Med J (Engl) 2007; 120:584-588.
10. Alster, TS., Tanzi, EL. Hypertrophic scars and keloids: etiology and management. Am J Clin Dermatol 2003; 4:235-243.
11. Harunari N, Zhu KQ, Armendariz RT, et al: Histology of the thick scar on the female, red Duroc pig: final similarities to human hypertrophic scar. Burns 2006; 32: 669-677.
12. Zhu KQ, Engrav LH, Gibran NS, et al: The female, red Duroc pig as an animal model of hypertrophic scarring and the potential role of the cones of skin. Burns 2003; 29: 649-664.
13. Zhu KQ, Engrav LH, Tamura RN, et al: Further similarities between cutaneous scarring in the female, red Duroc pig and human hypertrophic scarring. Burn 2004; 30:518-530.
14. Aksoy MH, Vargel I, Canter IH, et al: A new experimental hypertrophic scar model in guinea pigs. Aesthetic Plast Surg 2002; 26:388-396.
15. Liu W, Chua C, Wu X, et al: Inhibiting scar formation in rat wounds by adenovirus-mediated overexpression of truncated TGF-beta receptor II. Plast Reconstr Surg 2005; 115: 860-870.
16. Liu W, Mehrara BJ, Chin GS, et al: The use of newborn rats and an adenoviral

gene delivery vector as a model system for wound-healing research. Ann Plast Surg 2000; 44:543-551.

17. Kapoor M1, Howard R, Hall I, et al: Effects of epicatechin gallate on wound healing and scar formation in a full thickness incisional wound healing model in rats. Am J Pathol 2004; 165:299-307.
18. Colwell AS, Krummel TM, Kong W, et al: Skin wounds in the MRL/MPJ mouse heal with scar. Wound Repair Regen 2006; 14: 81-90.
19. Wilgus TA, Vodovotz Y, Vittadini E, et al: Reduction of scar formation in full-thickness wounds with topical celecoxib treatment. Wound Repair Regen 2003; 11:25-34.
20. Bloemen MC, van der Veer WM, Ulrich MM, et al: Prevention and curative management of hypertrophic scar formation. Burns 2009; 35:463-475.
21. Ogawa R, Mitsuhashi K, Hyakusoku H, et al: Postoperative electron-beam irradiation therapy for keloids and hypertrophic scars: retrospective study of 147 cases followed for more than 18 months. Plast Reconstr Surg 2003; 111: 547-553.
22. Murakami M, Ogawa R, Nishikawa M, et al: A rare case of hypertrophic scar on the scalp. Plast Reconstr Surg 2006; 117: 321-322.
23. Akaishi S1, Akimoto M, Ogawa R, et al: The relationship between keloid growth pattern and stretching tension: visual analysis using the finite element method. Ann Plast Surg 2008; 60: 445-451.
24. Wong VW, Beasley B, Zepeda J, et al: A Mechanomodulatory Device to

Minimize Incisional Scar Formation. Adv Wound Care (New Rochelle) 2013; 2(4):185-194.

25. Wong VW, Rustad KC, Akaishi S, et al: Focal adhesion kinase links mechanical force to skin fibrosis via inflammatory signaling. Nat Med 2011; 18(1):148-152.
26. Gurtner GC, Dauskardt RH, Wong VW, et al: Improving cutaneous scar formation by controlling the mechanical environment: large animal and phase I studies. Ann Surg 2011; 254(2) : 217-2.
27. Aarabi S, Bhatt KA, Shi Y, et al: Mechanical load initiates hypertrophic scar formation through decreased cellular apoptosis. FASEB 2007; 21(12):3250-3261.
28. Wu X, Gao Z, Song N, et al: Creating thick linear scar by inserting a gelatin sponge into rat excisional wounds. Wound Repair Regen 2007; 15: 595-606.
29. Wang J, Jiao H, Stewart TL, et al: Improvement in postburn hypertrophic scar after treatment with IFN-alpha2b is associated with decreased fibrocytes. J Interferon Cytokine Res 2007; 27: 921-930.
30. Huang C, Akaishi S, Hyakusoku H, et al: Are keloid and hypertrophic scardifferent forms of the same disorder? A fibroproliferative skin disorderhypothesis based on keloid findings. Int Wound J 2014;11(5):517-522.
31. Yang L, Scott PG, Giuffre J, et al: Peripheral blood fibrocytes from burn patients: identification and quantification of fibrocytes in adherent cells cultured from peripheral blood mononuclear cells. Lab Invest 2002;

82:1183-1192.

32. Tredget EE, Shankowsky HA, Pannu R, et al: Transforming growth factor-beta in thermally injured patients with hypertrophic scars: effects of interferon alpha-2b. Plast Reconstr Surg 1998; 102:1317-1328.
33. Kischer, CW., Bunce, H., Shetlah, MR. Mast cell analyses in hypertrophic scars, hypertrophic scars treated with pressure and mature scars. J Invest Dermatol 1978; 70:355-357.
34. Darby, IA., Hewitson, TD. Fibroblast differentiation in wound healing and fibrosis. Int Rev Cytol 2007; 257:143-179.
35. Hinz, B. Formation and function of the myofibroblast during tissue repair. J Invest Dermatol 2007; 127:526-537.
36. Hinz B, Phan SH, Thannickal VJ, et al: The myofibroblast: one function, multiple origins. Am J Pathol 2007; 170:1807-1816.
37. Tonnesen, MG., Feng, X., Clark, RA. Angiogenesis in wound healing. J Investig Dermatol Symp 2000; 5: 40-46.
38. Niessen FB1, Spauwen PH, Schalkwijk J, et al: On the nature of hypertrophic scars and keloids: a review. Plast Reconstr Surg 1999; 104:1435-1458.
39. MacKenna, D., Summerour, SR., Villarreal, FJ. Role of mechanical factors in modulating cardiac fibroblast function and extracellular matrix synthesis. Cardiovasc Res 2000; 46: 257-263.
40. Tetsunaga T, Nishida K, Furumatsu T, et al: Regulation of mechanical stress-induced MMP-13 and ADAMTS-5 expression by RUNX-2

transcriptional factor in SW1353 chondrocyte-like cells. Osteoarthritis Cartilage 2011; 19: 222-232.

41. Robinson JA, Chatterjee-Kishore M, Yaworsky PJ, et al: Wnt/beta-catenin signaling is a normal physiological response to mechanical loading in bone. J Biol Chem 2006; 281: 31720-31728.
42. Chin MS, Ogawa R, Lancerotto L, et al: In vivo acceleration of skin growth using a servo-controlled stretching device. Tissue Eng Part C Methods 2010 ;16(3):397-405.
43. Samuel MS, Lopez JI, McGhee EJ, et al: Actomyosin-mediated cellular tension drives increased tissue stiffness and beta-catenin activation to induce epidermal hyperplasia and tumor growth. Cancer Cell 2011; 19: 776-791.
44. Wang J, Jiao H, Stewart TL, et al: Accelerated wound healing in leukocyte-specific, protein 1-deficient mouse is associated with increased infiltration of leukocytes and fibrocytes. J Leukoc Biol 2007; 82: 1554-1563.
45. Wang J, Jiao H, Stewart TL, et al: Increased severity of bleomycin-induced skin fibrosis in mice with leukocyte-specific protein 1 deficiency. J Invest Dermatol 2008; 128: 2767-2776.
46. Tredget EE1, Nedelec B, Scott PG, et al: Hypertrophic scars, keloids, and contractures. The cellular and molecular basis for therapy. Surg Clin North Am 1997; **77:** 701-730.
47. Machesney M, Tidman N, Waseem A, et al: Activated keratinocytes in the epidermis of hypertrophic scars. Am J Pathol 1998; 152:1133-1141.

48. Niessen FB, Andriessen MP, Schalkwijk J, et al: Keratinocyte-derived growth factors play a role in the formation of hypertrophic scars. J Pathol 2001; 194: 207-216.

49. Lu L, Saulis AS, Liu WR, et al: The temporal effects of anti-TGF-beta1, 2, and 3 monoclonal antibody on wound healing and hypertrophic scar formation. J Am Coll Surg 2005; 201: 391-397.

50. Cowin AJ, Holmes TM, Brosnan P, et al: Expression of TGF-beta and its receptors in murine fetal and adult dermal wounds. Eur J Dermatol 2001; 11: 424-431.

51. Soo C, Hu FY, Zhang X, et al: Differential expression of fibromodulin, a transforming growth factor-beta modulator, in fetal skin development and scarless repair. Am J Pathol 2000; 157: 423-433.

52. Ferguson, MW., O'Kane, S. Scar-free healing: from embryonic mechanisms to adult therapeutic intervention. Philos Trans R Soc Lond B Biol Sci 2004; 359: 839-850.

53. van der Veer WM1, Bloemen MC, Ulrich MM, et al: Potential cellular and molecular causes of hypertrophic scar formation. Burns 2009; 35: 15-29.

Figure Legends

Figure 1. Rat HScs model and experimental design. (A) & (B): Two 2 cm linear full-thickness incisions (2cm apart) were made on the dorsum of the rat skin. Four clasps were sutured to each linear incision, with 2 on each side, 0.5cm apart from the incision. (Immediately after surgery) (C) A tensionmeter was used to measure the elastic tension. (D) Different tension driven modes were applied in different phase of wound healing. Group Control, E-ETD, LG-ETD, CG-ETD stand for the control group, the early tension group, the late gradient tension group and the continuous gradient tension group, respectively.

Figure 2. Finite element predicted tensile stress (A) and von Mises stress (B) distributions of the rat wounding skin/scar area, loaded with 0, 2, 3, 4, and 5N tensile force.

Figure 3. Gross view of scar widths in different groups at week 0, 1, 2, 4, and 8. The control group shows the narrowest scars and became invisible in week 4. In the E-ETD, LG-ETD, CG-ETD groups, the scars go the process similar to human scars. CG-ETD shows the widest scars than other groups.

Figure 4. H&E staining pictures (20 × and 100 ×) of the scar forming in each group. E-ETD, LG-ETD, CG-ETD show significantly larger scars formation as compared to

the control group. Yellow lines label the boundary of the scar areas.

Figure 5. Illustrative pictures for scar width, epidermal thickness measurement and scar width variation analysis. (A) Harvested scar tissues were cut at the middle, perpendicular to the incisional line. (B) a: the 2 black arrows indicate the epidermal thickness; b: indicates the scar width. (C) Scar width measurement of each group at 1w, 2w, 4w and 8w, respectivey. Data are expressed as the mean ± SD (n = 9, *p < 0.05).

Figure 6. Comparison of epidermis thickness in 4 groups. (A): The thickness of epidermis of the scar in 4 groups in week 4. (b) The growth status of the epidermis in each group at different time points. Data are expressed as the mean ± SD (n = 9, *p < 0.05).

Figure 7. Masson's Trichrome stain of the scar sections of each group 4 weeks after operation. Images were taken at 40 × magnification (the upper line) and 100 × magnification (the lower line), respectively. (Green color represents the staining for collagens.)

Figure 8. Immunohistochemical staining for TGF-β1 in the control group and the CG-ETD group. Photos were taken at 100 × magnification (the left two columns) and 400 × magnification (the right two columns) respectively.

Figure 9. Mast cell recruitment into the tension related scars. (A) shows the toludine blue staining for mast cells in scars at week 4 (400 × magnifications). (B) shows quantification of mast cells in scars of group A, B, C, D at different time points. Data are expressed as the mean ± SD (n = 9, *p < 0.05).

Figure 10. Comparison of the a-SMA-expressing cells and new blood vessel formation. (A) shows the a-SMA stain of normal rat skin incisional scars (the Control group) and the tension related scars (CG-ETD)at different time points at 40 × magnification; The red arrows indicate the a-SMA-expressing cells, the yellow arrows indicate the blood vessels formation. (B) shows the quantification of a-SMA-positive cells in the control group and CG-ETD at different time points; (C) shows the quantification of blood vessels in the control group and CG-ETD at different time points. (D) shows comparison of the a-SMA-expressing cells in group A and group D at high magnification (100 ×). The red arrows and the green circles indicate the a-SMA-expressing cells. (*$p < 0.05$, Data represent the mean ± SD, for n=9.)

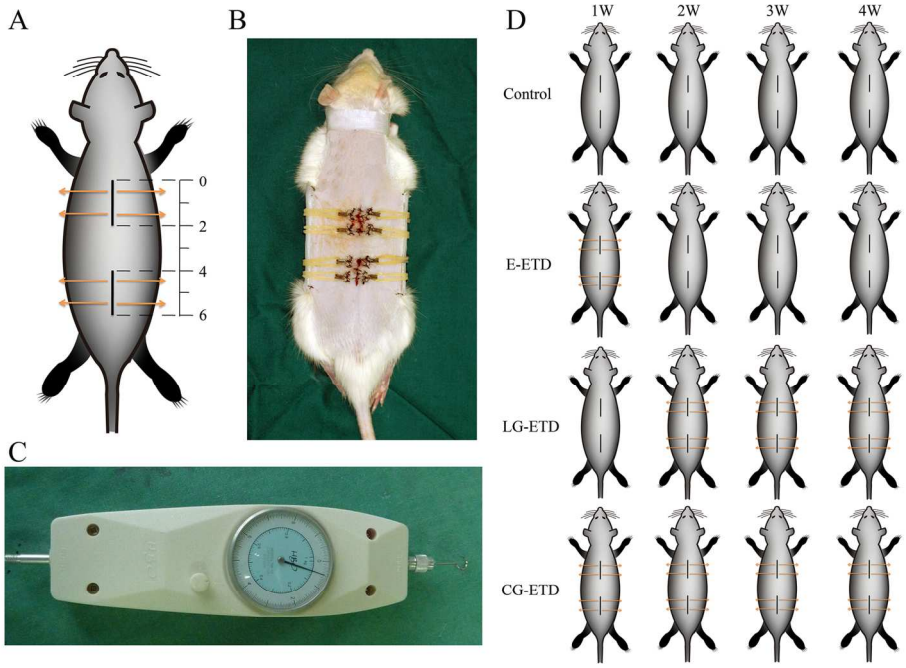

177x128mm (300 x 300 DPI)

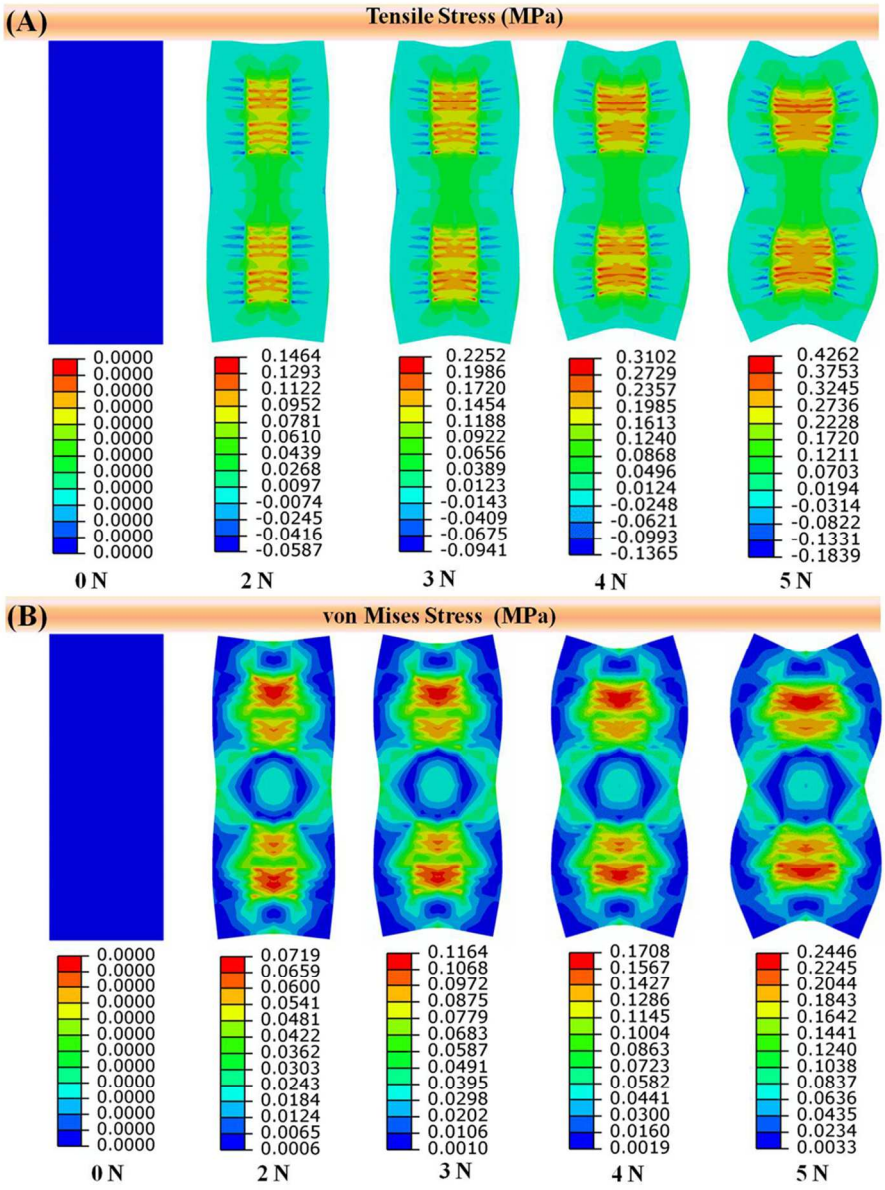

86x114mm (300 x 300 DPI)

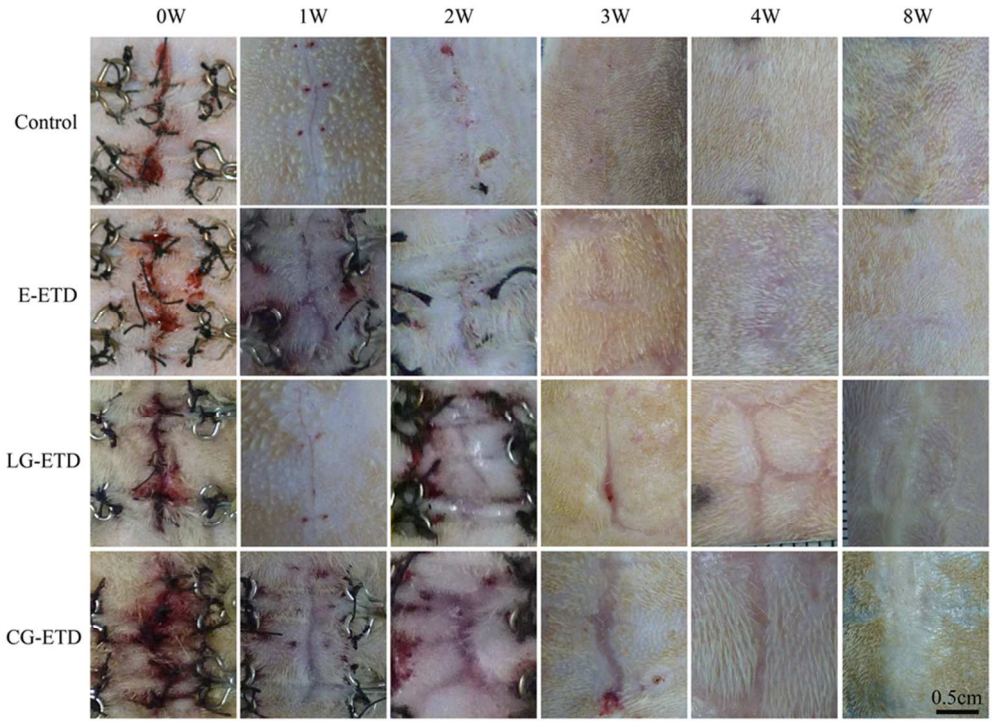

86x63mm (300 x 300 DPI)

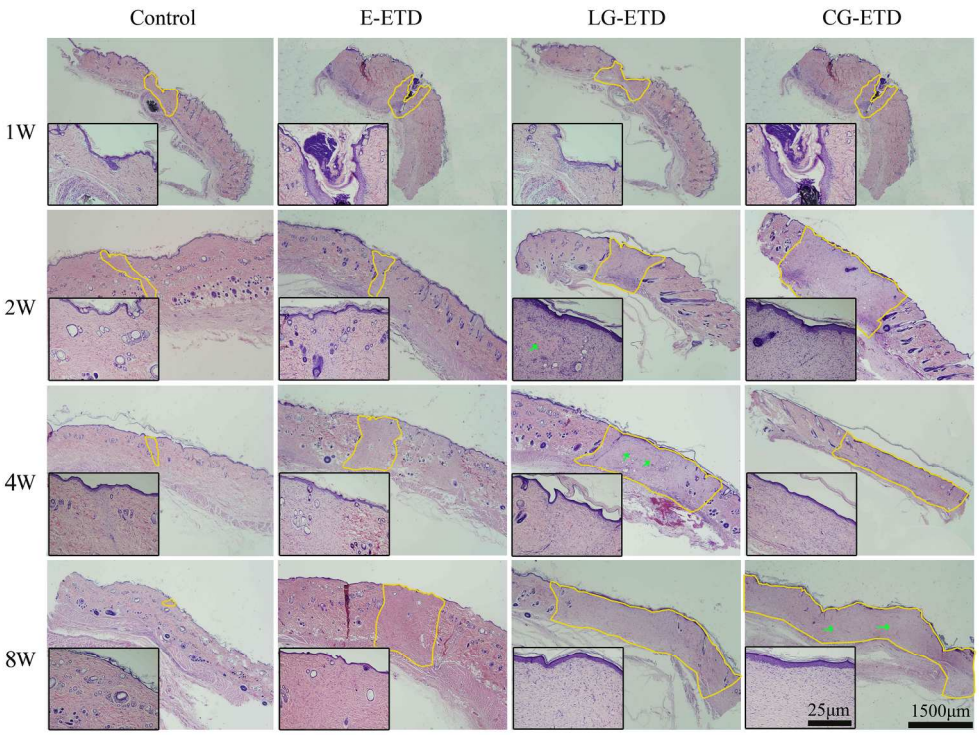
Control
E-ETD
LG-ETD
CG-ETD
1W
2W
4W
8W
25μm
1500μm

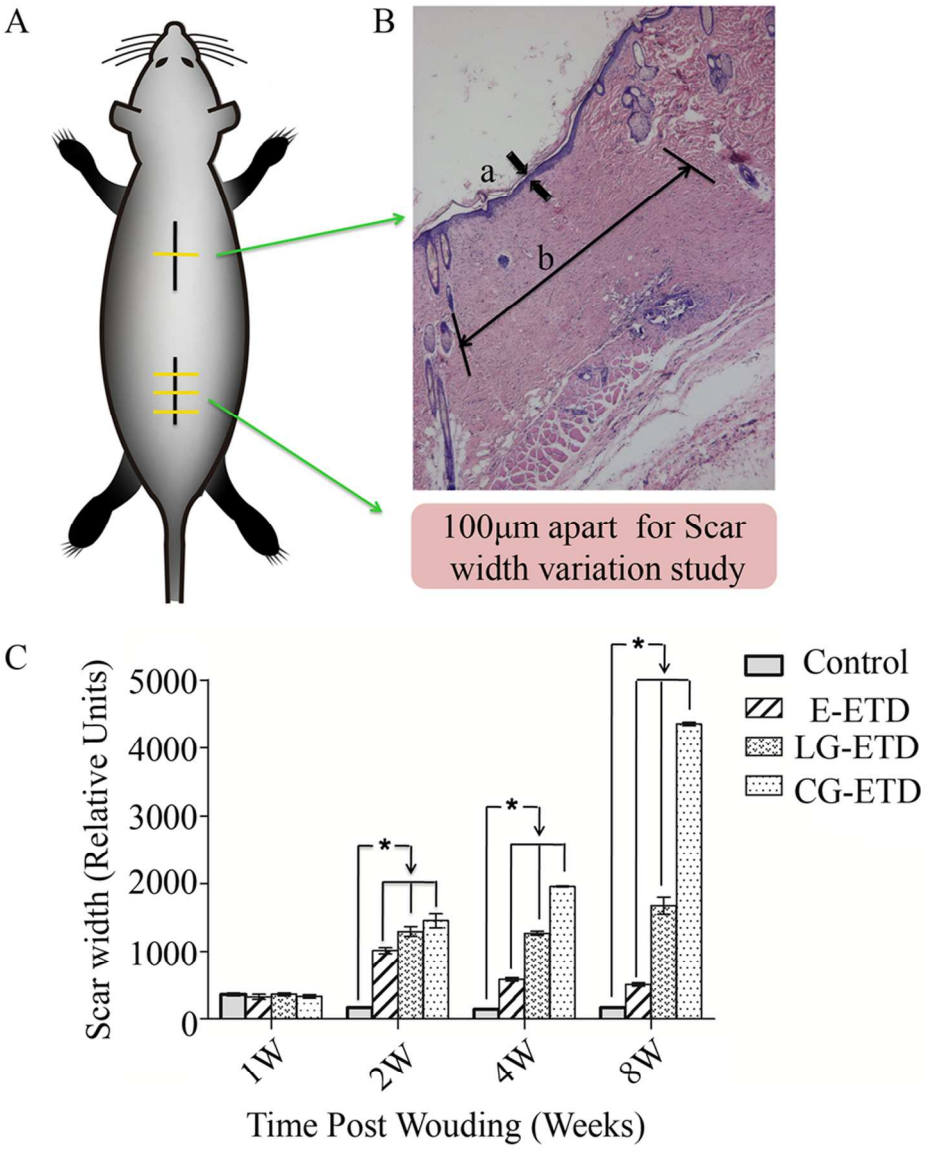
A
B
a
b
100μm apart for Scar width variation study
C
Scar width (Relative Units)
5000
4000
3000
2000
1000
0
1W
2W
4W
8W
Time Post Wouding (Weeks)
Control
E-ETD
LG-ETD
CG-ETD
*

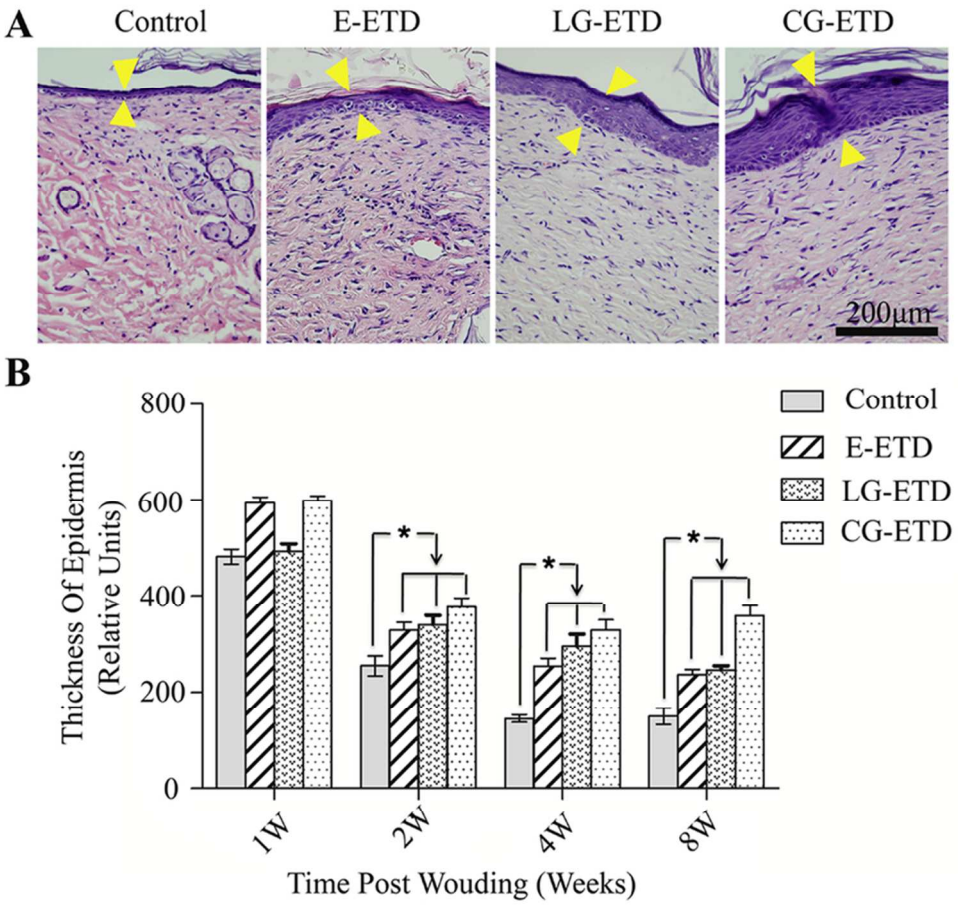

79x73mm (300 x 300 DPI)

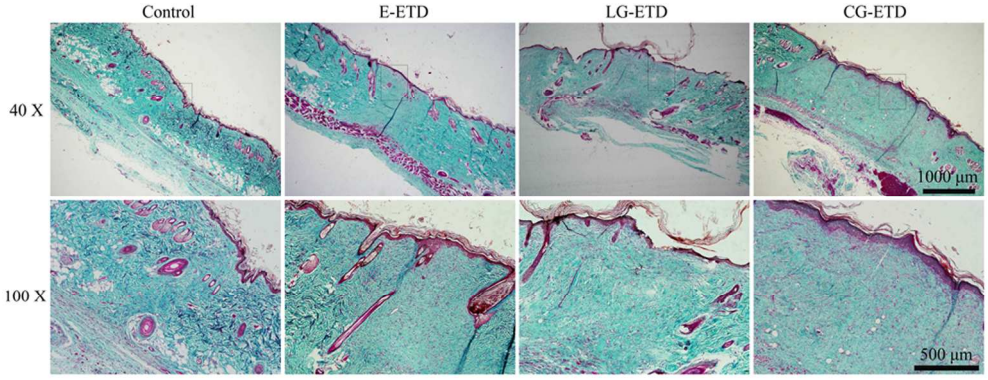
Control
E-ETD
LG-ETD
CG-ETD
40 X
100 X
1000 µm
500 µm

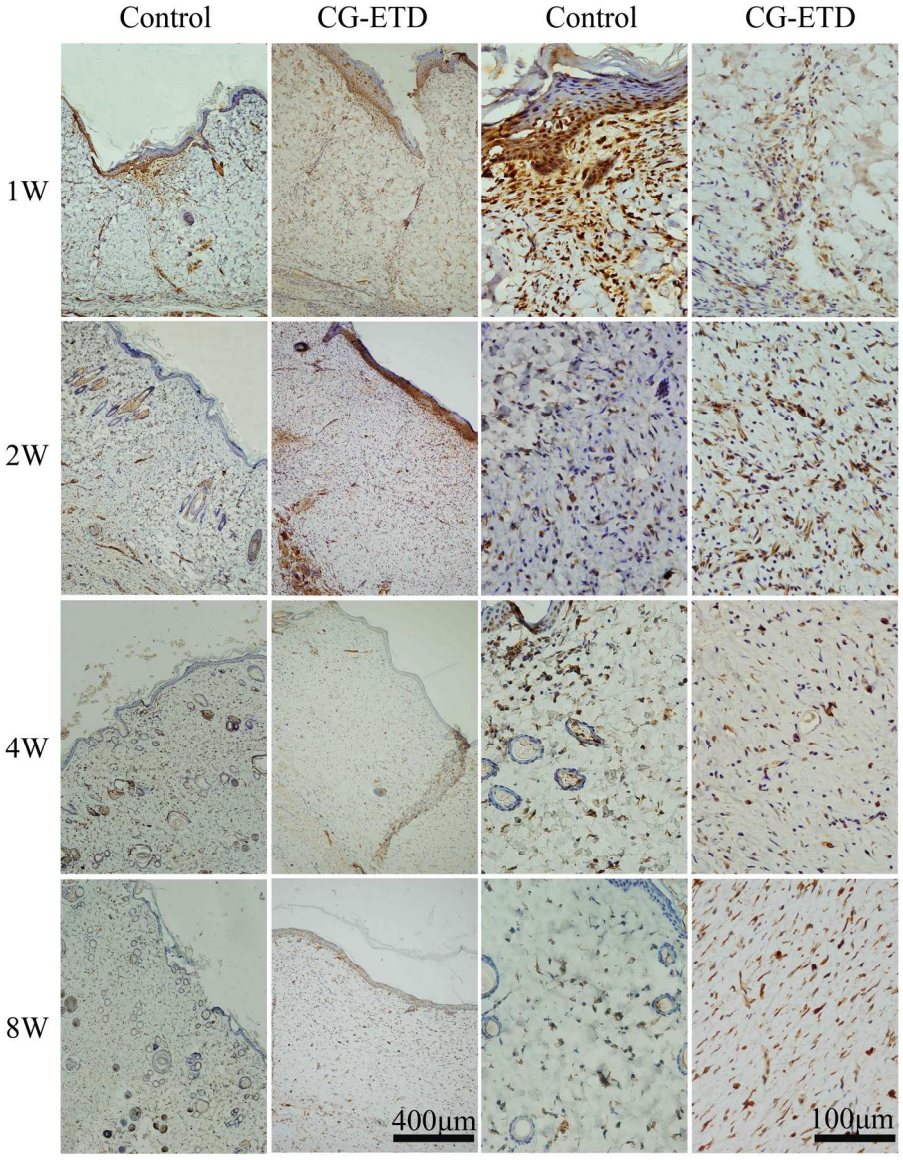
Control
CG-ETD
Control
CG-ETD
1W
2W
4W
8W
400μm
100μm

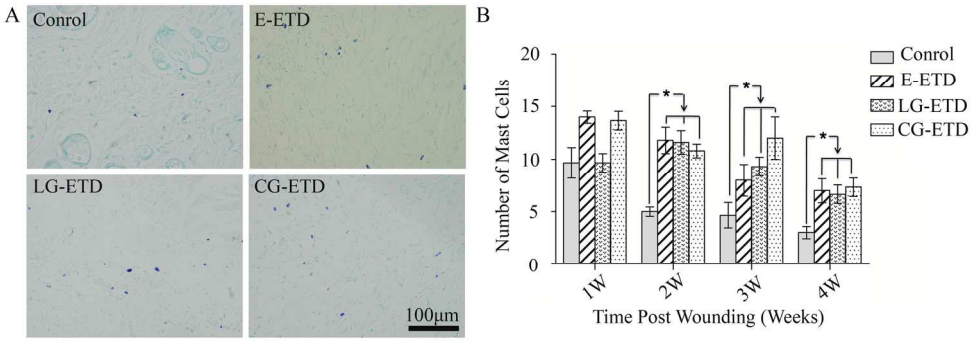

177x64mm (300 x 300 DPI)

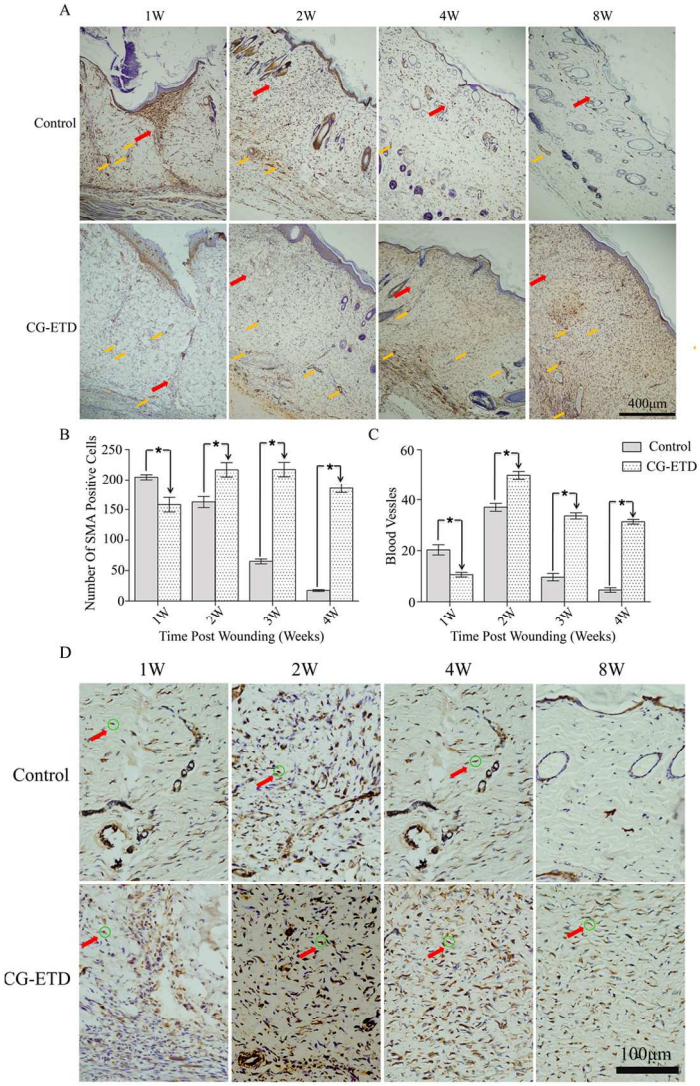
A
1W
2W
4W
8W
Control
CG-ETD
400μm
B
Number Of SMA Positive Cells
250
200
150
100
50
0
1W
2W
3W
4W
Time Post Wounding (Weeks)
C
Control
CG-ETD
Blood Vessles
60
40
20
0
1W
2W
3W
4W
Time Post Wounding (Weeks)
D
1W
2W
4W
8W
Control
CG-ETD
100μm